高等学校化学学报
CHEMICAL JOURNAL OF CHINESE UNIVERSITIES
综合评述

静电纺纳米纤维过渡金属基双功能电催化剂及其在全解水中的应用

银泳婷，卢晓峰
（吉林大学化学学院麦克德尔米德实验室，长春 130012）

摘要 电化学水分解是目前最具潜力的可持续制氢途径之一，然而，阴极析氢反应与阳极析氧反应所需的高过电位严重制约了其规模化应用. 过渡金属基催化剂因成本低、组成可调和具有类贵金属催化活性，可有效降低电极过电位，被视为替代贵金属催化剂的理想材料，因而备受关注. 本文总结了基于静电纺纳米纤维构筑的过渡金属双功能电催化剂的主要类型（金属、氧化物、磷化物、硫化物及碳化物等体系），重点讨论了提升其催化性能的关键策略（包括异质界面工程、杂原子掺杂、金属-非金属-金属桥接结构设计以及单原子位点调控等）. 最后，探讨了该领域面临的挑战与未来发展的方向，以期为高性能全解水电催化剂的理性设计与开发提供参考.

关键词 静电纺丝；纳米纤维；过渡金属基催化剂；全解水；性能优化
中图分类号 O636 **文献标志码** A doi：10.7503/cjcu20250280

Electrospun Nanofibrous Transition Metal-based Bifunctional Electrocatalysts Toward Overall Water Splitting

YIN Yongting, LU Xiaofeng*
(*Alan G. MacDiarmid Institute*, *College of Chemistry*, *Jilin University*, *Changchun* 130012, *China*)

Abstract Electrochemical water splitting represents a sustainable technology for hydrogen (H_2) production. However, its large-scale implementation is hindered by the high overpotentials required for both the cathodic hydrogen evolution reaction (HER) and the anodic oxygen evolution reaction (OER). Transition metal-based catalysts have garnered significant research interest as promising alternatives to noble-metal catalysts, owing to their low cost, tunable composition, and noble-metal-like catalytic activity. Nevertheless, systematic reviews on their application as bifunctional catalysts for overall water splitting (OWS) are still limited. This review comprehensively outlines the principal categories of bifunctional transition metal electrocatalysts derived from electrospun nanofibers (NFs), including metals, oxides, phosphides, sulfides, and carbides. Key strategies for enhancing their catalytic performance are systematically summarized, such as heterointerface engineering, heteroatom doping, metal-nonmetal-metal bridging architectures, and single-atom site design. Finally, current challenges and future research directions are discussed, aiming to provide insightful perspectives for the rational design of high-performance electrocatalysts for OWS.

Keywords Electrospinning; Nanofibers; Transition metal-based catalyst; Overall water splitting; Performance optimization

收稿日期：2025-09-29. 网络首发日期：2025-12-02.
联系人简介：卢晓峰，男，博士，教授，主要从事纳米纤维材料方面的研究. E-mail：xflu@jlu.edu.cn
基金项目：国家自然科学基金（批准号：52273056）和吉林省科技厅项目（批准号：YDZJ202501ZYTS305）资助.
Supported by the National Natural Science Foundation of China(No. 52273056) and the Science and Technology Development Program of Jilin Province, China(No.YDZJ202501ZYTS305).

1 Introduction

With the ever-growing global energy demand and progressively stringent environmental requirements, developing renewable and clean energy systems has become a worldwide priority. The finite availability of traditional fossil fuels, together with the carbon emissions and environmental pollution caused by their consumption, highlights the urgent need to transform the current energy infrastructure. Hydrogen(H_2) energy, recognized as an efficient and renewable clean energy source, is widely regarded as a pivotal alternative to fossil fuels due to its zero-carbon emission characteristic, as its sole combustion product is water. Current primary H_2 production technologies include steam methane reforming, partial oxidation of hydrocarbons, and water electrolysis. Among these, water electrolysis, which utilizes water as the sole feedstock and produces no polluting emissions, is recognized as one of the most environmentally benign pathways for generating green H_2[1]. Water electrolysis technology employs electrical energy to drive the decomposition of water into H_2 and oxygen(O_2), with the core reactions being the hydrogen evolution reaction(HER) at the cathode and the oxygen evolution reaction(OER) at the anode. Nevertheless, a significant challenge of this process lies in its high energy consumption[2]. The OER, in particular, suffers from high charge transfer resistance, leading to an actual operating voltage(typically 1.8—2.0 V) that substantially exceeds the theoretical thermodynamic equilibrium potential of 1.23 V, thereby requiring a considerable overpotential. The design of highly active and stable electrocatalysts represents a crucial pathway to effectively lower the reaction overpotentials and enhance the overall energy conversion efficiency[3].

Currently, noble-metal-based materials(*e.g.*, Pt for HER, Ir, IrO_2, and RuO_2 for OER) remain the benchmark electrocatalysts for water electrolysis. However, their widespread implementation is constrained by high cost, limited reserves, and insufficient long-term stability. In recent years, substantial research efforts have been directed toward developing low-cost and durable transition metal-based alternatives[4]. By forming composites, the electrochemical performance of these catalysts has been further improved[5]. Extensive investigations have covered a wide range of systems, including transition metals and their alloys, oxides, phosphides, sulfides, nitrides, and carbides. Notably, some of these catalysts exhibit excellent bifunctional activity for both HER and OER, rivaling or even approaching the performance of noble-metal benchmarks, thereby demonstrating promising application potential[6]. Transition metal-based catalysts demonstrate prominent advantages in HER/OER catalytic systems, which can be summarized as follows: (1) diverse phase composition. A single transition metal can form various phases, including oxides, phosphides, sulfides, nitrides, and carbides. This diversity provides a versatile material platform for catalytic reactions. (2) Highly tunable electronic structure. Strategies such as alloying, heteroatom doping and phase engineering enable precise modulation of key electronic parameters(*e.g.*, *d*-band center, e_g orbital occupancy, coordination environment). This tunability optimizes the adsorption behavior of reaction intermediates by adjusting the hydrogen adsorption free energy(ΔG_{H^*}) for HER close to the ideal value(*ca.* 0 eV) and lowering the energy barrier of the rate-determining step(RDS) in OER, thereby significantly enhancing electrocatalytic activity. (3) Tailorable microstructure. These materials can be engineered into diverse morphologies, such as one-dimensional(1D) nanowires, multidimensional ordered arrays, and hollow/core-shell structures. These designed architectures effectively increase the density of exposed active sites while promoting mass transport and reinforcing structural stability.

Among various nanostructured materials, 1D nanomaterials have demonstrated significant potential in electrocatalytic water splitting due to their unique properties, such as directional electron transport and efficient mass transfer[7]. In particular, nanofibrous materials fabricated *via* electrospinning have attracted

considerable attention owing to their highly tunable architectures and flexible composition design compared to the particle-shaped catalysts[8]. This technique enables the precise construction of diverse fiber morphologies, including solid, hollow, core-shell, multi-channel, Janus, and hierarchical structures[9]. Moreover, it allows for the controllable synthesis of nanofibers (NFs) with various compositions, such as carbon-based, metallic, ceramic, and their composites. These electrospun NFs exhibit exceptional electrocatalytic performance for the HER, OER, and overall water splitting (OWS). Furthermore, electrospinning offers a versatile route for the controllable fabrication of self-supported catalytic membranes. This strategy eliminates the use of polymer binders typically required in traditional electrode preparation, thereby significantly enhancing electrical conductivity and mechanical stability, which lays a solid foundation for practical applications. This review systematically summarizes recent advances in electrospun NFs-based materials for OWS, as illustrated in Fig. 1. We begin by outlining the fundamental principles of electrospinning and the structural characteristics of the resultant NFs, followed by a discussion of the design principles governing their use as electrocatalysts. We then categorize and critically evaluate the OWS performance of various types of electrospun NFs catalysts, with special emphasis on performance-enhancement strategies based on structural engineering and electronic modulation. Finally, we present a perspective on the current challenges and future research directions in this field, aiming to accelerate the translation of electrospun NFs-based electrocatalysts from fundamental research to practical application.

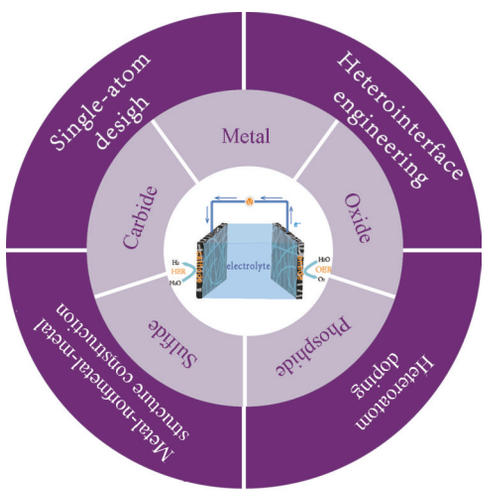


Fig. 1 Scheme for the electrospun nanofibrous transition metal-based bifunctional electrocatalysts toward OWS

2 Electrospinning Technology and Nanofibrous Materials

2.1 Fundamentals of Electrospinning Technology

Electrospinning is a versatile and scalable technique for the continuous fabrication of micro- to nano-scale fibers from polymer solutions or melts using a high-voltage electrostatic field[10]. In a typical process, a polymer or its precursor is dissolved in a suitable solvent to form a spinnable solution with appropriate viscosity and conductivity. Upon applying a high voltage between the syringe nozzle and the collector, electrostatic repulsion among the surface charges of the droplet causes it to deform into a conical shape known as a Taylor cone. Once the electric field force exceeds the surface tension of the liquid, a charged jet is ejected from the cone tip. This jet subsequently undergoes substantial stretching and thinning, driven by the electrostatic forces and rapid solvent evaporation, ultimately solidifying into continuous solid NFs that deposit on the collector. During the electrospinning process, the morphology and microstructure of the resulting NFs are governed by three main categories of factors: solution properties, processing parameters, and ambient conditions. Regarding solution properties, an excessively low viscosity tends to cause droplet formation instead of continuous fibers, while overly high viscosity hinders jet elongation. A lower surface tension facilitates stable jet formation and can be modulated using surfactants or cosolvents. Polymer concentration also plays a critical role in influencing the morphology and structure of polymer NFs. A lower concentration

generally favors the formation of finer fibers, whereas a higher concentration increases fiber diameter and may cause nozzle clogging. Additionally, the solvent evaporation rate must be moderate; overly rapid evaporation can induce bead formation, while excessively slow evaporation may result in incomplete drying and solvent retention. Concerning processing parameters, the applied voltage is typically set within the range of 5—30 kV. Increasing the voltage generally enhances fiber refinement, though excessively high voltage can cause jet instability or splitting. The feed rate also affects fiber morphologies, a higher rate tends to increase fiber diameter and may lead to spindle-like structures or intermittent dripping-jetting. The tip-to-collector distance must be optimized in relation to the electric field strength to balance jet stretching and solvent evaporation. Among ambient conditions, elevated temperature reduces solution viscosity and accelerates solvent evaporation. High humidity levels can promote the formation of porous fiber surfaces by interfering with evaporation kinetics, whereas air currents may disturb the jet path and compromise process stability. Therefore, the reproducible preparation of NFs with uniform morphology and stable structure requires systematic optimization and synergistic control of all the aforementioned parameters.

2.2 Design Principles for Electrospun NFs as Bifunctional Electrocatalysts

Employing bifunctional HER and OER catalysts for OWS simplifies the electrolyzer structure, reduces manufacturing costs, and improves overall system stability. To realize their application for OWS, they must exhibit excellent activities for both HER and OER. HER is a cathodic process involving a two-electron transfer, and its reaction pathway typically follows either the Volmer-Tafel or Volmer-Heyrovsky mechanism[11,12]. Although the pathways differ, both critically depend on the catalyst′s ability to adsorb hydrogen intermediates (H^*). Consequently, the key to designing efficient HER catalysts centers on optimizing the H^* adsorption strength, with the ΔG_{H^*} serving as the primary activity descriptor. Optimal HER performance is generally achieved when the ΔG_{H^*} approaches zero. To date, a diverse range of HER electrocatalysts based on electrospun NFs have been developed, including noble metals, transition metals and their alloys, oxides, phosphides, sulfides, and carbides[13]. These materials demonstrate significant potential for optimizing adsorption behavior through electronic structure modulation. In contrast, the OER is a four-electron-transfer anodic process characterized by sluggish kinetics[12]. It typically requires a high overpotential to proceed and often acts as the RDS in OWS. Thus, developing efficient OER catalysts is crucial for enhancing the overall efficiency of water electrolysis. While RuO_2 and IrO_2 have long served as benchmark OER catalysts, their high cost, scarcity, and limited operational stability have motivated extensive research for alternatives[14]. Transition metal-based electrocatalysts (*e. g.*, alloys, oxides, phosphides, sulfides, carbides, and hydroxides) are regarded as promising substitutes due to their low cost, abundance, and tunable catalytic properties[15]. The OER performance of these materials can be significantly enhanced by optimizing the adsorption energies of key reaction intermediates (*e.g.*, O^*, OH^*, OOH^*), which in turn lowers the energy barrier of the RDS.

In summary, the rational design of electrospun NFs-based bifunctional catalysts for OWS should adhere to the following principles. First, the electronic structure of the material should be optimized through compositional engineering to precisely regulate the adsorption energies of HER/OER intermediates, thereby minimizing the reaction energy barriers of the RDS. Second, a continuous 1D conductive network with hierarchical porosity facilitates efficient electron transport and mass diffusion, contributing to the enhanced electrocatalytic performance. Furthermore, the structural versatility of electrospun NFs could be fully leveraged to engineer specific fiber morphologies (*e. g.*, hollow, core-shell, or Janus structures), which increases the exposure of active sites and enhances mechanical stability. Ultimately, a synergistic balance between high catalytic activity and long-term operational durability must be achieved to ensure efficient and

stable performance under practical OWS conditions.

3 Electrospun Nanofibrous Transition Metal-based Electrocatalysts for OWS

In contrast to noble-metal-based catalysts, transition metal-based electrocatalysts offer the advantages of abundant resource availability and lower cost. Furthermore, they encompass a greater diversity of materials, including not only transition metals and their alloys but also oxides, phosphides, sulfides, and carbides. After electrospinning into the nanofibrous morphology, they exhibit exceptional HER and OER properties, which are promising for practical OWS applications.

3.1 Transition Metals and Alloys

Transition metal alloys are widely employed in the HER, OER, and OWS, due to their high catalytic activity, tunable electronic structures, excellent selectivity, and remarkable stability[16—21]. For instance, although Ru-based catalysts are recognized as excellent bifunctional electrocatalysts, they often suffer from dissolution or over-oxidation during operation, leading to performance degradation. Alloying Ru with Au at the atomic level has been demonstrated to effectively enhance both its catalytic activity and stability[22]. Studies show that AuRu alloy NFs prepared *via* an electrospinning-calcination-reduction method require overpotentials of only 43 mV for HER and 154 mV for OER to achieve a current density of 10 mA/cm^2 in acidic media. Density functional theory (DFT) calculations reveal that the ΔG_{H^*} on the AuRu alloy is closer to the ideal value of 0 eV compared to pure Ru, indicating that the incorporation of Au weakens the hydrogen adsorption on Ru sites, thereby boosting the HER activity. When configured as a two-electrode OWS system, it requires a cell voltage of only 1.438 V to deliver 10 mA/cm^2, outperforming the benchmark Pt/C‖Ir/C couple.

Recently, the controllable synthesis of bimetallic Co-Ir NFs was successfully achieved through a combination of electrospinning, a two-step heat treatment, and a galvanic replacement reaction [Fig.2(A)][23]. Scanning electron microscopy (SEM) image confirmed the uniform 1D nanofibrous morphology of the material [Fig.2(B)]. Transmission electron microscopy (TEM) image further revealed a rough fiber surface with a distinct core-shell-like structure, indicating that the replacement reaction primarily occurred on the surface of the Co fiber templates [Fig.2(C)]. X-ray diffraction (XRD) patterns indicated that the catalyst is primarily composed of a CoIr alloy and metallic Co. The presence of clear interfaces between CoIr and Co particles was visible in high-resolution TEM (HRTEM) image [Fig.2(D)], which was further corroborated by selected-area electron diffraction (SAED) pattern, confirming the co-existence of CoIr alloy and Co crystalline phases [Fig.2(E)]. Benefiting from the unique 1D nanofibrous architecture and the synergistic electronic effect between the Ir and Co components, the catalyst exhibited outstanding OER activity in an alkaline electrolyte, requiring an overpotential of only 169 mV at a current density of 10 mA/cm^2 with a Tafel slope of 46.7 mV/dec [Fig.2(F)—(H)]. It also demonstrated notable HER performance [Fig.2(I)—(K)]. When employed as both the anode and cathode in a two-electrode alkaline electrolyzer, the system required a cell voltage of only 1.51 V to achieve 10 mA/cm^2 and exhibits excellent durability, outperforming the benchmark Pt/C‖IrO_2 couple and most reported OWS systems. This study provides a versatile and efficient preparation strategy for developing cost-effective and high-performance metal-based electrocatalysts for OWS.

Electrochemical water splitting in strongly acidic or alkaline environments can cause severe material corrosion, whereas neutral conditions are milder and more conducive to enhancing catalyst durability. Using electrospinning combined with a carbonization process, NiCo bimetallic nanoparticles can be encapsulated within nitrogen-doped carbon (NC) NFs, forming a NiCo@NC composite catalyst[24]. After optimization of the carbonization temperature, this catalyst demonstrated excellent bifunctional activity for both HER and OER in

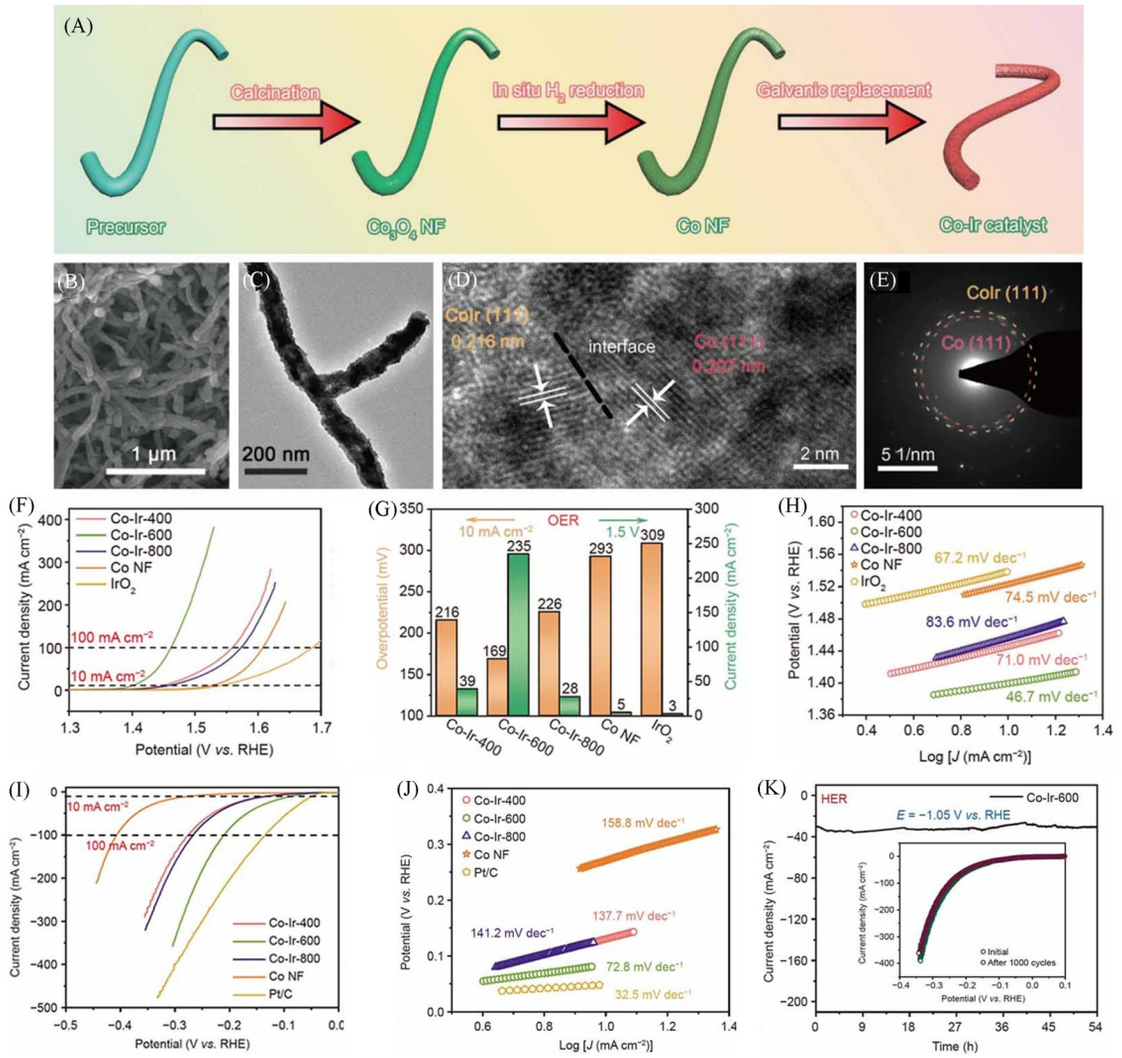


Fig. 2 Scheme of the procedure to prepare the Co-Ir nanofibrous catalyst(A), SEM image(B), TEM image (C), HRTEM image(D) and SAED pattern(E) of the Co-Ir-600 NFs, LSV curves of varied electrocatalysts for OER(F), comparison of OER activity for varied catalysts(G), Tafel slopes of varied catalysts for OER(H), LSV curves(I) and Tafel slopes(J) of varied catalysts for HER and *i-t* curve and the LSV curves before and after 1000 CV cycles(inset) of Co-Ir-600 NFs for HER(K)[23]

Copyright 2023, Science China Press.

a neutral buffer solution, requiring overpotentials of only 126. 7 mV for HER and 396 mV for OER at a current density of 10 mA/cm^2. The material possessed a high specific surface area, which facilitates the exposure of more active sites. Concurrently, the encapsulated structure of the nanoparticles effectively prevented the aggregation, leaching, and electrolyte corrosion of the NiCo species during the reaction, significantly improving structural stability. Furthermore, the electronic synergy between the Ni and Co metals further optimized the adsorption behavior of reaction intermediates, enhancing the intrinsic catalytic activity.

3.2 Transition Metal Oxides

Transition metal oxides hold great promise as bifunctional electrocatalysts for OWS, capable of simultaneously driving both the HER and OER, owing to their tunable electronic structures and abundant active sites[25]. Their catalytic activity originates from the multi-valent transition capability of metal ions and the presence of oxygen vacancies, which collectively optimize the adsorption energies of key reaction intermediates. Through strategic nanostructural design and compositional engineering, the electrical

conductivity and structural stability of transition metal oxides can be further enhanced, leading to a significant reduction in the voltage for OWS. This provides a viable pathway for efficient and low-cost renewable energy conversion.

Recently, our group has successfully synthesized ruthenium-cobalt oxide($RuCoO_x$) solid-solution NFs *via* electrospinning followed by air calcination. This material demonstrates exceptional bifunctional catalytic performance for both HER and OER at industrial-level current densities[26]. The study revealed a strong composition-dependent activity. The Ru_2CoO_x NFs exhibited optimal OER activity, requiring an overpotential of only 362 mV to achieve 1000 mA/cm^2, while the $RuCoO_x$ NFs showed superior HER performance, with an overpotential as low as 149 mV at the same current density. A two-electrode OWS electrolyzer was constructed using $RuCoO_x$ as the cathode and Ru_2CoO_x as the anode($RuCoO_x$‖Ru_2CoO_x)[Fig.3(A)]. This system required a cell voltage of only 1.48 V to reach 10 mA/cm^2, which is considerably lower than that of the Pt/C‖RuO_2 benchmark system(1.69 V)[(Fig.3(B) and (C)] and outperforms most reported bifunctional electrocatalysts [Fig.3(D)]. Remarkably, the system achieved Faradaic efficiencies(FEs) close to 100% for both HER and OER at 200 mA/cm^2[Fig.3(E) and (F)], indicating excellent energy conversion efficiency. Chronoamperometry tests[Fig.3(G)] confirmed outstanding stability, with the electrolyzer operating steadily for over

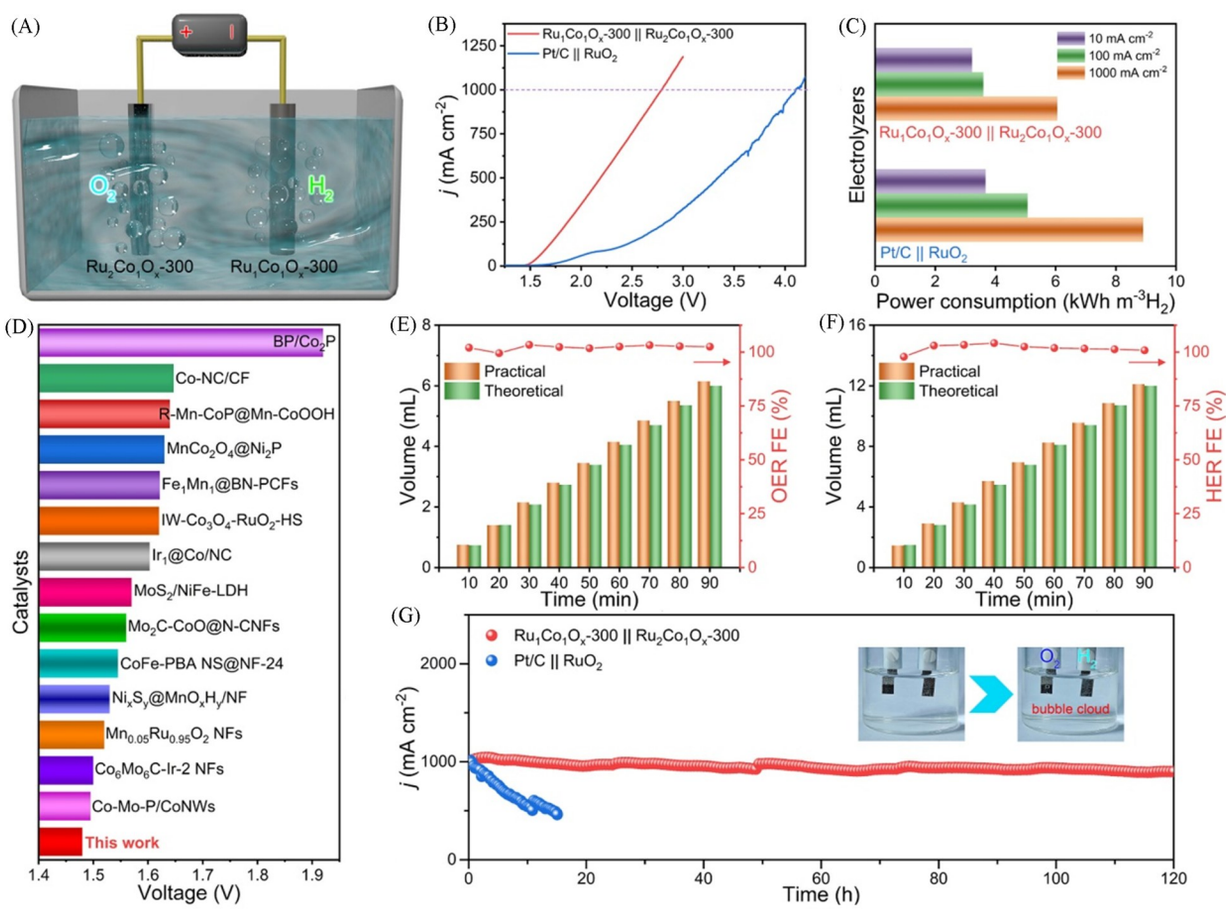


Fig. 3 Schematic illustration of the alkaline two-electrode OWS system(A), LSV curves without iR correction(B) and power consumption for H_2 generation at various current densities in two electrolysis systems(C), comparison of voltages at 10 mA/cm^2 among various electrolysis systems(D), practical and theoretical O_2(E) and H_2(F) production as well as the FEs of the OWS system, stability test and the gas bubbles at the electrodes in the electrolyte(inset) of $RuCoO_x$-300‖Ru_2CoO_x-300 and Pt/C‖RuO_2 electrolysis systems(G)[26]

Copyright 2025, Elsevier.

120 h at a high current density of 1000 mA/cm^2, significantly outperforming the Pt/C‖RuO_2 system. The vigorous evolution of H_2 and O_2 bubbles on the electrode surfaces was visually observed during operation[inset in Fig. 3(G)]. These results collectively demonstrate that the $RuCoO_x$ solid-solution NFs catalysts possess remarkable catalytic activity and durability under industrial-grade operating conditions, highlighting their significant potential for practical water electrolysis applications.

3.3 Transition Metal Phosphides

Transition metal phosphides have demonstrated significant advantages in electrocatalytic water splitting due to their low cost, tunable structures, good electrical conductivity, and noble-metal-like electronic properties[27—30]. Currently, NaH_2PO_2 is a commonly used phosphorus source for the preparation of metal phosphides. For instance, Chang *et al.*[31] successfully synthesized CoMoP NFs by phosphorizing electrospun $CoMoO_4$ NFs precursors with NaH_2PO_2 at elevated temperatures. The resulting material exhibited excellent bifunctional catalytic activity for both HER and OER. Although transition metal phosphides show high activity for HER and OER, their practical performance is often limited by issues such as poor particle dispersion, low specific surface area, and insufficient electronic conductivity. To overcome these disadvantages, researchers have designed hierarchical cobalt phosphide/carbon NFs(CoP/C NFs) composites[32]. This material leverages the synergy between CoP nanosheets and a 1D C NFs network, which provides abundant active sites and facilitates rapid electron/mass transport. It requires overpotentials of only 325 mV for OER and 225 mV for HER to achieve a current density of 10 mA/cm^2. When assembled into an OWS system, it requires a cell voltage of only 1.65 V to reach 10 mA/cm^2. Chen *et al.*[33] further proposed a "dual-confinement" strategy to construct metal phosphides/carbon composite. On one hand, utilizing the pores of metal-organic framework (MOF)-derived carbon to confine the growth of phosphide particles, and on the other hand, enhancing stability through the spatial constraint of polyacrylonitrile (PAN) fibers[33]. This strategy resulted in the $CoNiP_x$-C NF catalyst featuring a smaller particle size, more active sites, and phosphorus vacancies. Simultaneously, the introduced metal-N coordination optimized the electronic structure, and the bimetallic synergistic effect reduced the overpotentials for HER and OER in alkaline electrolyte to 154 and 269 mV at 10 mA/cm^2, respectively. When employed as a self-supported electrode for OWS, the system required a voltage of only 1.56 V at 10 mA/cm^2 and demonstrated exceptional stability.

Beyond NaH_2PO_2, phytic acid(PA) can serve as an effective phosphorus source to modulate the composition of phosphides and prevent particle agglomeration. Liu *et al.*[34] utilized phytic acid as both a chelating agent and a phosphorus source, and combined with oxidized coal to enhance mechanical strength, to fabricate NiCoP nanoparticles embedded within coal-based C NFs(denoted as NiCoP@C-C NFs-2). This self-supported bifunctional catalyst required overpotentials of only 121 mV for HER and 259 mV for OER at a current density of 10 mA/cm^2. This high performance is attributed to the PA-induced uniform distribution of nanoparticles and the exposure of highly active sites. In OWS test, the system achieved a cell voltage of 1.636 V at 10 mA/cm^2, maintained stable operation for 50 h, and exhibited an FE close to 100%, demonstrating an excellent integration of high activity, remarkable stability, and structural flexibility.

3.4 Transition Metal Sulfides

Transition metal sulfides are widely employed as electrocatalysts for water electrolysis due to their high intrinsic activity, large specific surface area, and unique electrochemical properties[35,36]. Compared to metal oxides, sulfides generally possess a narrower band gap and higher electron mobility. Their surfaces are prone to form unsaturated coordination atoms, which can serve as highly efficient active centers to enhance the adsorption and activation of reaction intermediates. Furthermore, sulfides can be uniformly deposited on substrates such as carbon materials, which helps improve the overall structural stability. For example, an

amorphous bimetallic sulfide, NiFeS, can be electrodeposited onto the surface of Co-C NFs to form a Co-C/NiFeS composite electrocatalyst [Fig. 4 (A)][37]. SEM and TEM images revealed that NiFeS grew uniformly on the surface of the Co-C NFs in the form of nanosheets [Fig.4(B) and (C)], and the thickness of the deposited layer could be controllably tuned by varying the electrodeposition time. HRTEM image confirmed the amorphous nature of the NiFeS layer [Fig. 4 (D)]. Raman spectroscopy provided further verification of the successful synthesis of NiFeS. Specifically, new characteristic peaks observed near 354

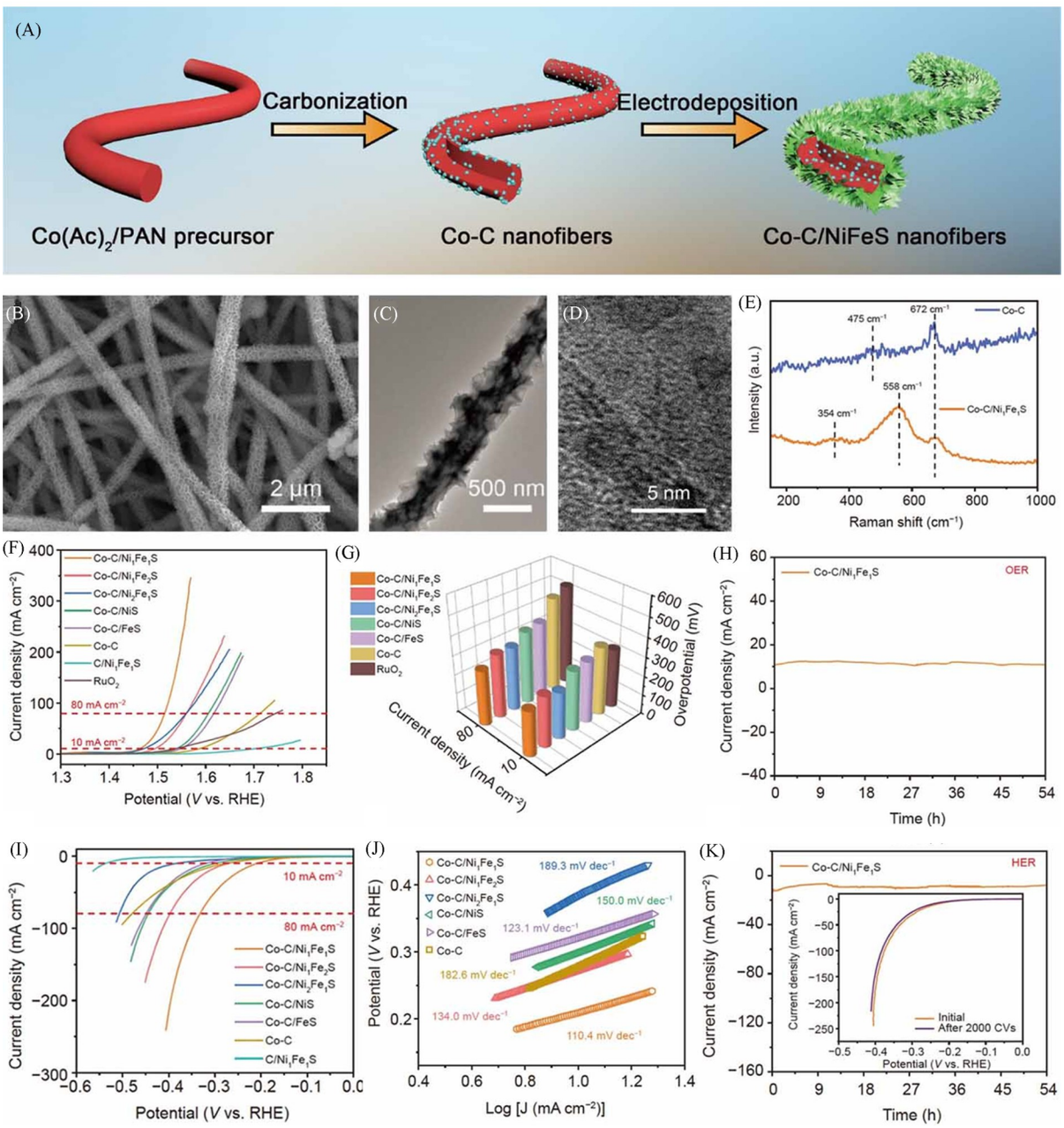


Fig. 4 Illustration of the preparation process of Co-C/NiFeS NFs(A), SEM(B), TEM(C), HRTEM(D) images of Co-C/NiFeS NFs, Raman spectra of Co-C and Co-C/NiFeS NFs(E), LSV curves of varied electrocatalysts for OER(F), collections of overpotentials at 10 and 80 mA/cm^2(G), OER durability at around 10 mA/cm^2(H) of Co-C/NiFeS NFs, LSV curves(I) and Tafel slopes(J) of varied electrocatalysts for HER and *i-t* curve and the LSV curves before and after 2000 CV cycles(inset) of Co-C/NiFeS NFs for HER(K)[37]

Copyright 2023, Science China Press.

and 558 cm^{-1} in the Co-C/NiFeS sample were assigned to the stretching vibrations of the Fe—S and Ni—S bonds, respectively[Fig.4(E)]. In an alkaline electrolyte, the catalyst exhibited excellent OER and HER performance. As shown in Fig.4(F) and (G), it required an OER overpotential of only 233 mV to achieve a current density of 10 mA/cm^2, which is significantly lower than that of the monometallic NiS and FeS sulfides supported on Co-C NFs, as well as the NiFeS control sample supported on bare carbon fibers. This catalyst also presented a favorable OER durability over 54 h[Fig.4(H)]. Simultaneously, its HER overpotential and Tafel slope were also significantly lower than those of the control materials[Fig.4(I) and (J)], along with a desirable long-term stability[Fig.4(K)]. The performance enhancement is attributed to the synergistic effect of the composite architecture. The crystalline Co nanoparticles embedded within the carbon fibers provide highly conductive pathways, while the amorphous NiFeS nanosheets contribute a high specific surface area and abundant active sites. Leveraging the bifunctional nature of Co-C/NiFeS, three different alkaline electrolyzer configurations were constructed. Among them, the Pt/C||Co-C/NiFeS system required a cell voltage of only 1.48 V at 10 mA/cm^2, while the symmetric Co-C/NiFeS||Co-C/NiFeS system demonstrated the best stability, retaining 92.9% of its initial current density after 70 h of continuous operation.

3.5 Transition Metal Carbides

Transition metal carbides have garnered extensive attention in the field of water electrolysis due to their high electrical conductivity and superior intrinsic activity[38—42]. Among them, molybdenum-based carbides are regarded as "platinum-like catalysts" or "non-precious metal analogues of Pt" because of their Pt-like *d*-band electronic structure. However, the Mo—H bond formed between the *d*-orbital vacancies of Mo and hydrogen intermediates is excessively strong, which impedes H_2 desorption. Therefore, optimizing their H^* adsorption/desorption behavior through electronic structure modulation is crucial for enhancing HER performance. Similarly, rational electronic structure engineering is also beneficial for lowering the energy barrier of the RDS in OER. Based on this understanding, researchers developed a bimetallic WMo carbide NFs as a bifunctional HER/OER catalyst[43]. This material possesses a uniform nanofibrous morphology and a hydrophilic surface(contact angle of 59.6°), which is conducive to electrolyte penetration and reaction mass transport. Electrochemical tests confirmed its excellent activity for both HER and OER. When assembled into an anion exchange membrane electrolyzer, the system achieved a current density of 100 mA/cm^2 at a voltage of only 1.82 V and maintained stable operation for 100 h even at a high current density of 200 mA/cm^2, demonstrating promising potential for practical application. DFT calculations were employed to further elucidate the contribution of the electronic structure to the catalytic activity. As shown in Fig.5(A), the difference in work function between W and Mo carbides promotes the formation of a built-in electric field at their interface, facilitating rapid electron transfer. Bader charge analysis indicated electron transfer from Mo_2C to WC_{1-x}[Fig.5(B)]. The energy barriers for each step of the HER process are presented in Fig.5(C) and (D). The water dissociation energy barriers at the W and Mo sites were as low as 0.302 and 0.312 eV, respectively, significantly lower than those on monometallic carbides, indicating that the bimetallic synergy effectively promotes water dissociation kinetics. Fig.5(E) and (F) show the adsorption configurations of three key intermediates during OER and the corresponding free energy diagrams on the catalyst surface, revealing that the W site acts as the primary active center with superior activity, thereby enhancing the reaction kinetics. Projected density of states(PDOS) analysis[Fig.5(G)] showed an upshift of the *d*-band center for Mo and a downshift for W, resulting in an overall moderate *d*-band center. This adjustment weakens the overly strong adsorption of intermediates and optimizes the reaction energy barriers[Fig.5(H) and (I)]. This precise modulation of the electronic structure is identified as the key mechanism for enhancing the bifunctional activity for both HER and OER.

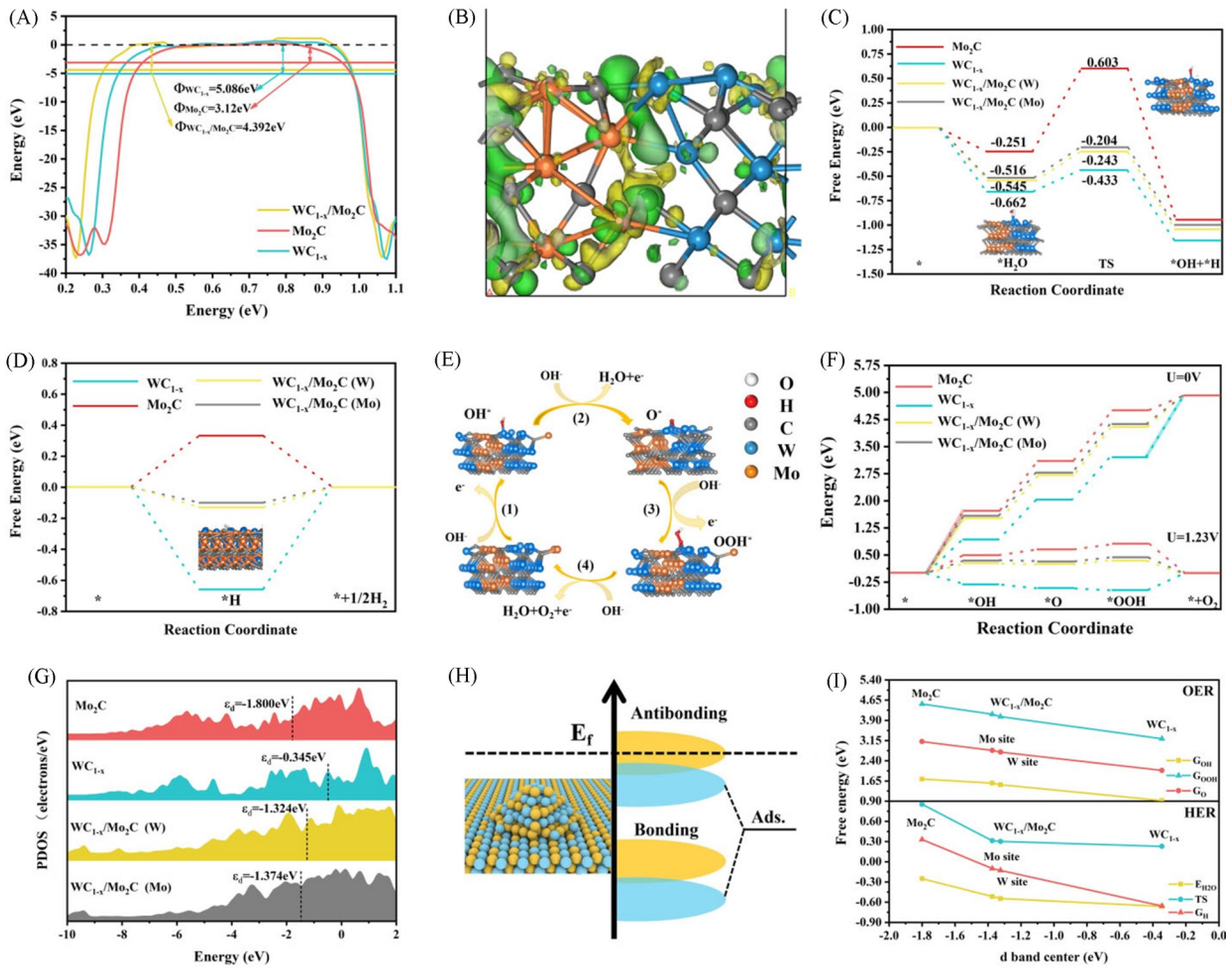


Fig. 5 DFT calculation results of WC_{1-x}/Mo_2C, Mo_2C and WC_{1-x}[43]

(A) Calculated work function; (B) deformation charge density of catalyst; (C) calculated adsorption and dissociation energies of H_2O on the catalysts; (D) computed Gibbs free energy; (E) proposed pathways for OER; (F) adsorption free energy of oxygen-containing intermediates on the catalysts; (G) the *d*-band centers of Mo and W; (H) schematic diagram illustrating the correlation between the *d*-band center and adsorption strength; (I) comparison of the free energy of key intermediates *versus* *d*-band center positions. Copyright 2024, John Wiley and Sons.

4 Strategies for Enhancing the OWS Performance of Electrospun Nanofibrous Transition Metal-based Electrocatalysts

The performance of an electrocatalyst in water splitting is governed by multiple factors, including the adsorption capability, density, and intrinsic activity of the active sites, as well as the desorption behavior of reaction intermediates. These properties are largely determined by the catalyst's morphology, size, microstructure, and electronic characteristics. Consequently, both the chemical composition and electronic structure of a catalyst have a decisive influence on its HER, OER, and OWS performance. Current strategies for enhancing the performance of transition metal-based electrocatalysts primarily focus on controlled structural engineering, which mainly encompasses the following aspects: the construction of heterogeneous interfaces, heteroatom doping, the design of metal-nonmetal-metal bridge bonds, and single-atom catalyst engineering.

4.1 Heterogeneous Interface Engineering

The construction of heterogeneous interfaces is a pivotal strategy for enhancing the performance of electrocatalysts[44—53]. Integrating multiple functional components to form heterostructures can not only introduce dual or even multiple active sites but also holistically optimize the overall properties of the catalyst. The chemical

coupling between different components generates a synergistic effect, which subsequently modulates the material's structure, exposes more active sites, and enhances the adsorption/desorption capabilities for reaction intermediates, ultimately leading to a significant boost in catalytic activity. A representative study involved the construction of a Mott-Schottky heterojunction electrocatalyst *via* an electrospinning-carbonization strategy, which anchored Ni/CeO_2 nanoparticles onto nitrogen-doped C NFs (Ni/CeO_2@N-CNFs)[54]. This heterojunction effectively triggered a self-driven charge transfer at the interface, increased the charge migration rate, and optimized the adsorption energy of reaction intermediates, thereby significantly accelerating the reaction kinetics. Experiments demonstrated that Ni/CeO_2@N-C NFs exhibited excellent bifunctional activity for both HER and OER in an alkaline electrolyte, requiring overpotentials of only 100 and 230 mV, respectively, at a current density of 10 mA/cm^2. When assembled into an OWS electrolyzer, it required a cell voltage of only 1.56 V to achieve 10 mA/cm^2 and demonstrated long-term stability for over 55 h.

Recently, our group constructed a novel heterostructured bifunctional electrocatalyst, termed Co_6Mo_6C-Ir NFs, by anchoring iridium(Ir) nanoparticles onto the surface of Co_6Mo_6C NFs bridged by nitrogen-doped carbon[55]. This catalyst simultaneously exhibited excellent activity and stability for both HER and OER in an alkaline medium. With a low Ir loading of only 5.9%(mass fraction), the Co_6Mo_6C-Ir NFs required remarkably low overpotentials of 348 mV for HER and 316 mV for OER at a high current density of 1 A/cm^2 and maintained stable operation for over 500 h at ampere-level current densities. The underlying mechanism for the high performance was elucidated by DFT calculations. Charge density difference analysis revealed multi-pathway electron transfer within the Co_6Mo_6C-Ir system, including Ir→C/N→Mo and Co→C/N→Mo routes[Fig.6(A)], where Ir, Co, and Mo atoms act as electron donors and N atoms as electron acceptors. This synergistic electronic modulation effectively activated the catalytic activity of C and Ir atoms, significantly enhancing HER performance. The ΔG_{H^*} values for some Ir-associated bridge and hollow sites were close to zero, confirming their excellent intrinsic HER activity. On the other hand, while the top site of an Ir cluster(T_{Ir1}) showed a high OER overpotential(1.90 V), the Ir atoms bonded to N/C at the interface (Ir_2-Ir_4) exhibited a reduced electron density, which weakened the adsorption strength of oxygen-containing intermediates and lowered the overpotential to 0.49—0.91 V[Fig.6(B) and (C)]. An alkaline electrolyzer assembled based on this catalyst required a cell voltage of only 2.79 V to achieve 1 A/cm^2, with FEs of 97.6% for HER and 99.0% for OER, significantly outperforming the Pt/C‖IrO_2 benchmark system[Fig.6(D) and (E)]. The electrolyzer also exhibited a low activation potential and demonstrated exceptional stability for 500 h at the industrial-grade current density of 1 A/cm^2, highlighting its great potential for practical application [Fig.6(F) and (G)]. Similarly, Zhao *et al.*[56] fabricated Co_3O_4/Bi_2MoO_6 heterojunction nanotubes *via* electrospinning followed by calcination. This material demonstrated superior HER and OER activity compared to its individual components. DFT calculations revealed that a built-in electric field formed at the heterointerface drives electron transfer from Bi_2MoO_6 to Co_3O_4, thereby significantly enhancing the electrocatalytic performance.

Core-shell heterostructures can effectively modulate the *d*-band center of catalysts *via* the built-in electric field formed at the interface, thereby optimizing the adsorption energy of reaction intermediates. This architecture not only enables simultaneous electronic structure regulation but also significantly enhances the material's stability and catalytic activity. Zhu *et al.*[57] designed a core-shell structure with Co_9S_8 as the core and MoS_2 as the shell, supported on C NFs, forming a Co_9S_8@MoS_2/C NFs composite material. This material exhibited low overpotentials for both HER and OER, significantly outperforming the single-component Co_9S_8/C NFs and MoS_2/C NFs catalysts. The excellent performance originates from the synergistic effect between Co and Mo at the interface of Co_9S_8 and MoS_2, which promotes electron transfer between the two phases. DFT

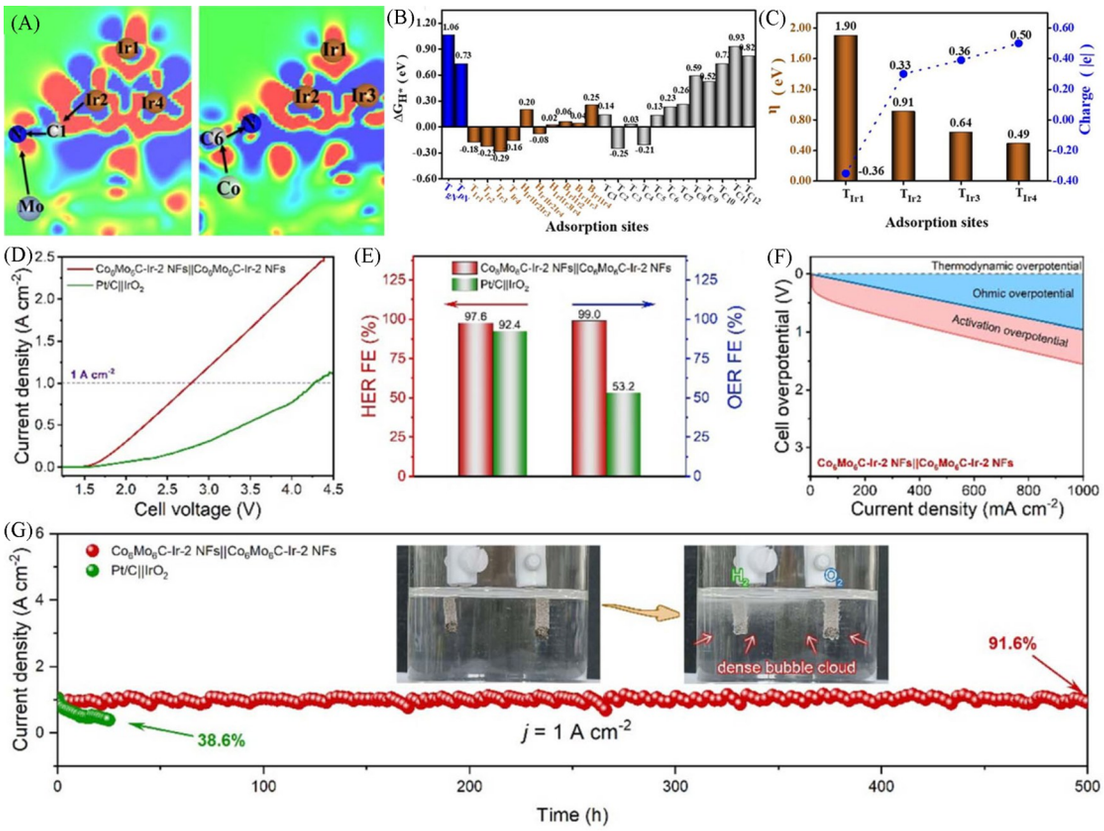


Fig. 6 Charge density difference of Co_6Mo_6C-Ir NFs catalyst(A), ΔG_{H^*} at varied adsorption sites(B), OER overpotentials on Co_6Mo_6C-Ir NFs and Bader charge of various active sites(C), polarization curves of two electrolyzers(D), FEs of the two electrolyzers measured at 200 mA/cm^2(E), the ohmic and activation overpotential analysis for Co_6Mo_6C-Ir-2 NFs||Co_6Mo_6C-Ir-2 NFs system(F) and the long-term stability test and the vigorous generation of H_2 and O_2 at the electrodes(insets) of two electrolyzers(G)[55]

Copyright 2024, the Royal Society of Chemistry.

calculations further revealed that the core-shell interface significantly reduces the kinetic energy barrier for the H_2 desorption process, thereby effectively enhancing the electrocatalytic performance. Furthermore, the fabricated Co_9S_8@MoS_2/C NFs membrane possesses self-supporting characteristics and can be directly used as a working electrode, laying a foundation for its practical application in electrocatalytic water splitting.

4.2 Heteroatom Doping

Heteroatom doping is a simple yet effective strategy for modifying electrocatalysts, leading to significant performance enhancement[58—60]. This approach modulates the electronic structure of the catalyst, optimizes the adsorption energy of reaction intermediates, and introduces new active centers. It creates a multi-component synergistic effect at the atomic scale, thereby boosting catalytic activity. The doping elements, which include metal atoms(*e.g.*, Ni, Co, Fe) and non-metal atoms(*e.g.*, N, S, P), are crucial for the performance improvement. Electrospinning technology, owing to its high compositional tunability, facilitates the precise incorporation of heteroatoms into metal compounds, allowing for the regulation of the coordination environment and electronic structure to achieve remarkable catalytic performance enhancement.

Our group constructed multivalent Mn-doped RuO_2($Mn_xRu_{1-x}O_2$) NFs *via* an electrospinning-calcination strategy[61]. The study found that optimizing the Mn doping level could significantly enhance the HER and OER activity of RuO_2 NFs at industrial-grade current densities. In an alkaline medium, the optimized

$Mn_{0.05}Ru_{0.95}O_2$ NFs required overpotentials of only 269 mV for HER and 461 mV for OER at 1 A/cm^2, and demonstrated long-term stability for 500 h and 170 h, respectively, outperforming commercial Pt/C and RuO_2 catalysts. DFT calculations revealed that Mn doping effectively modulates the electronic structure of RuO_2. The top site of an oxygen atom (O1) near Mn exhibited high HER activity due to its near-zero ΔG_{H^*} value (0.18 eV), which is much lower than those at other adsorption sites[Fig.7(A) and (B)]. Furthermore, we observed that the O1 atom retains a lone pair after forming two Ru—O bonds and one Mn—O bond. Upon H^* adsorption at this site, a fully occupied bonding orbital ($\sigma_{O—H}$) and a partially filled antibonding orbital ($\sigma^*_{O—H}$) were formed[Fig.7(C)], thereby weakening the O—H bond strength. Concurrently, significant electron transfer between O1 and its adjacent Ru/Mn atoms further enhanced the antibonding character and weakened the O—H bond, ultimately enabling optimal ΔG_{H^*} at this site. For OER, the system exhibited low overpotentials of 0.38 V at the T_{Mn} site and 0.46 V at the T_{Ru} site near Mn[Fig.7(D)], both lower than that of

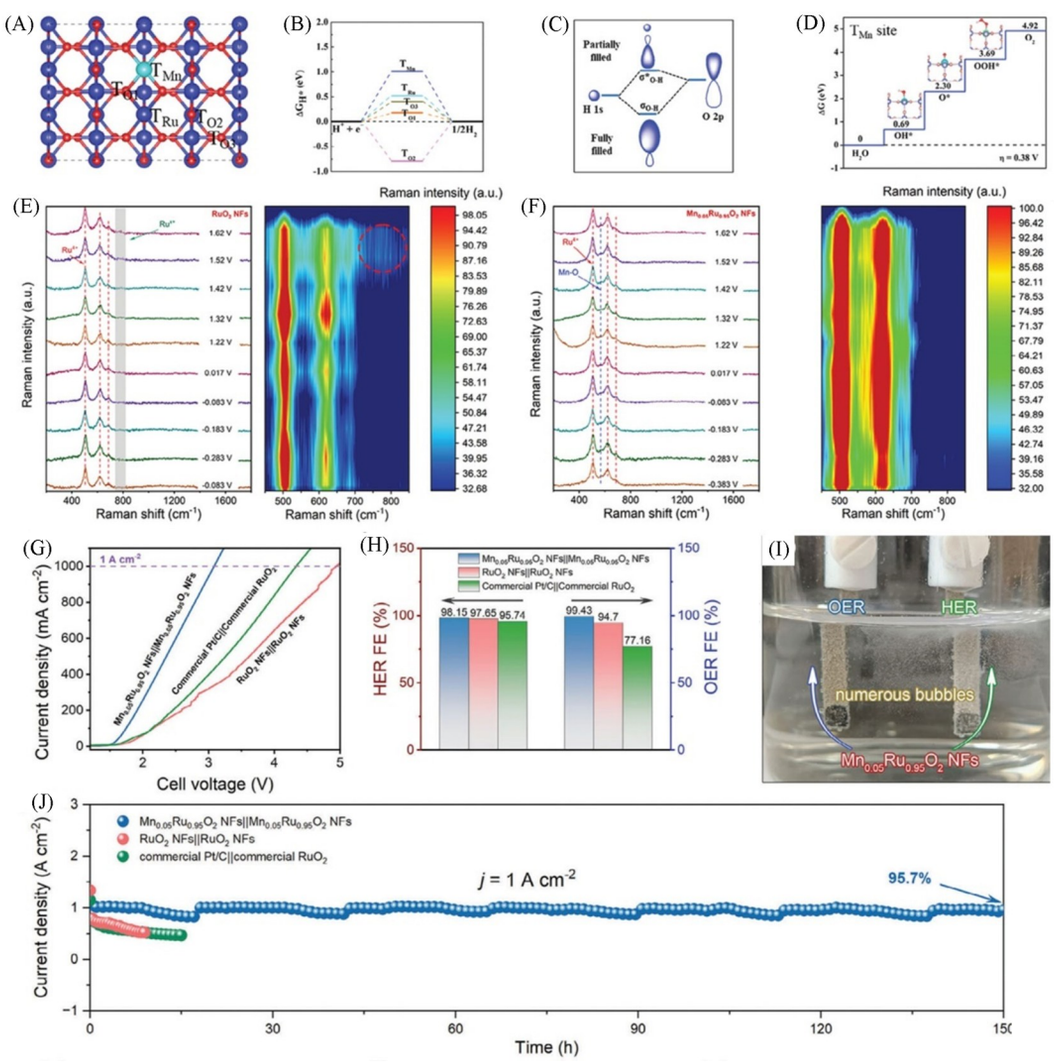


Fig. 7 Adsorption sites for H^* on Mn-doped RuO_2(A), the calculated ΔG_{H^*} at varied adsorption sites(B), schematic illustration of the formed fully filled bonding orbital and a partially filled antibonding orbital for H^* adsorption(C), free energy diagram of OER at the top site of Mn in Mn-doped RuO_2 (D), potential-dependent Raman spectra of RuO_2 NFs Mn-doped RuO_2 NFs(E, F), LSV curves(G) and FEs(H) of various electrolysis systems, digital photograph for generating H_2 and O_2 bubbles at cathode and anode(I) and the stability test of various electrolysis systems(J)[61]

Copyright 2024, John Wiley and Sons.

pristine RuO_2(0.53 V), demonstrating that Mn doping significantly enhances the OER catalytic performance of the RuO_2 system. To investigate the stability enhancement mechanism, potential-dependent Raman spectroscopy was performed[Fig.7(E) and (F)]. Compared to pure RuO_2 NFs, the Mn-doped sample showed no characteristic peak for high-valence Ru^{x+}(x>4) at *ca.* 785 cm^{-1}, suggesting effective suppression of high-valence Ru formation during OER. Inductively coupled plasma(ICP) results further confirmed that Mn doping significantly inhibited Ru dissolution during both HER and OER. A $Mn_{0.05}Ru_{0.95}O_2$||$Mn_{0.05}Ru_{0.95}O_2$ electrolyzer assembled based on this material required a cell voltage of only 1.52 V to achieve 10 mA/cm^2 for OWS, with FEs of 98.15% for HER and 99.43% for OER[Fig.7(G)—(I)]. It maintained excellent stability over 150 h of continuous operation[Fig.7(J)], significantly surpassing the performance of the commercial Pt/C||RuO_2 benchmark and most reported high-performance electrolyzers.

Compared to metal doping, non-metal elements offer advantages such as abundant reserves, low cost, and simpler doping processes. Furthermore, they tend to form strong covalent bonds with the host material, making them less prone to leaching or degradation under high potentials and in acidic/alkaline environments. Consequently, they have emerged as promising alternatives to precious metal dopants. For example, incorporating non-metallic phosphorus(P) into RuO_2 NFs significantly enhanced their alkaline electrocatalytic activity for OWS[62]. Interestingly, P doping induced the formation of a dendritic structure, effectively increasing the number of active sites. DFT calculations indicated that P doping modulates the position of the Ru *d*-band center, optimizing the adsorption energy of reaction intermediates and thereby significantly enhancing HER activity. For the OER process, the introduction of P not only optimized the adsorption behavior of intermediates but also lowered the reaction activation energy, leading to improved OER performance. An alkaline OWS electrolyzer constructed with this catalyst required a cell voltage of only 1.52 V to achieve 10 mA/cm^2 and operated stably for 100 h at a high current density of 1 A/cm^2. Its overall performance surpassed that of the Pt/C||RuO_2 benchmark and most reported water electrolysis systems. Similarly, Surendran *et al.*[63] doped sulfur(S) atoms into a Co-NiO heterostructure supported on nitrogen-enriched C NFs, inducing electron rearrangement. The S doping introduced an asymmetric charge density distribution within the carbon matrix, enhancing its electronic conductivity and thereby further boosting the catalytic activity.

Beyond metal oxides, other transition metal compounds such as phosphides, sulfides, and carbides can also have their electrocatalytic performance enhanced through doping strategies. Taking transition metal phosphides as an example, although they possess good catalytic activity and durability, their overall performance generally remains inferior to that of noble-metal-based catalysts. Introducing heterometallic atoms to modulate their composition can effectively improve their intrinsic activity. Liu *et al.*[64] successfully prepared a composite material with iron-doped cobalt phosphide nanoparticles anchored within C NFs(denoted as Fe-CoP/NCNF) through a multi-step process involving electrospinning, carbonization, air calcination, and phosphidation. The study demonstrated that regulating the air calcination temperature effectively tuned the porous structure of the fibers and the exposure degree of metal sites, thereby enhancing the electrocatalytic performance. The optimized catalyst exhibited excellent bifunctional activity for both HER and OER under alkaline conditions, requiring overpotentials of 159 and 292 mV, respectively, at a current density of 10 mA/cm^2. The performance enhancement is primarily attributed to the following factors: (1) iron doping optimized the intrinsic catalytic properties of the CoP nanoparticles; (2) the three-dimensional C NFs network facilitated electron transport and reactant mass transfer; (3) the abundant porous structure exposed more active sites. When assembled into an OWS electrolyzer, it required a cell voltage of only 1.63 V to achieve a current density of 10 mA/cm^2, demonstrating promising application potential.

4.3 Construction of Metal-nonmetal-metal Bridge Bonds

The electrocatalytic activity of transition metal oxides is closely related to their electronic structure. Recently, optimizing the electronic structure by constructing metal-nonmetal-metal bridge bonds has become a key strategy for enhancing HER and OER performance[65]. Li *et al.*[66] proposed a hetero-lattice engineering strategy, constructing a Co—O—Mo interface within a bimetallic CoMo oxide for bifunctional OWS catalysis. Synchrotron-based X-ray absorption spectroscopy(XAS) analysis indicated significantly enhanced electron transfer kinetics at the Co—O—Mo interface, contributing to exceptional HER performance. DFT calculations revealed that the Co—O—Mo interface possesses a lower ΔG_{H^*} compared to the Mo sites in pure MoO_3. Furthermore, the Mo sites at this interface exhibited a low water dissociation energy barrier in alkaline media, ensuring a continuous supply of H^*, resulting in an ultra-low HER overpotential of 40 mV at 10 mA/cm^2, superior to commercial Pt/C. Concurrently, interfacial lattice distortion induced by the lattice mismatch between the two oxides caused Co^{3+} ions to transition from a low-spin state to a high-spin state. PDOS analysis confirmed a significantly enhanced spin-polarized state of the Co *d*-band near the Fermi level in Co—O—Mo compared to Co_3O_4. The high-spin configuration thermodynamically optimized the adsorption behavior of oxygen intermediates, reducing the OER overpotential to 211 mV at 10 mA/cm^2, outperforming commercial RuO_2(321 mV). Leveraging its excellent bifunctional properties, the catalyst was assembled into an anion exchange membrane electrolyzer. This system required a cell voltage of only 1.48 V at 10 mA/cm^2, lower than the RuO_2||20%Pt/C benchmark system(1.58 V). The FEs for both H_2 and O_2 were close to 100%, indicating highly efficient energy conversion. In terms of stability, the electrolyzer operated stably for over 200 h at 10 mA/cm^2, outperforming most reported bifunctional catalyst systems. It also exhibited rapid response and sustained stable output at various current densities, demonstrating excellent potential for practical application.

Beyond oxygen-bridged structures, other non-metal elements such as boron(B) can fulfill similar functions. With an electronegativity of 2.04 on the Pauling scale, B possesses both electron-donor/acceptor characteristics, enabling effective modulation of the coordination environment and redistribution of the electron density in the host material. Bridging two metal atoms *via* B can synergistically activate the metal sites, enhancing electrocatalytic performance for both HER and OER. Recently, our group successfully constructed a novel Ru—B—Cr structure by co-introducing B and Cr atoms into RuO_2 NFs[67]. SEM and TEM images confirmed the nanofibrous morphology with a rough surface and an average diameter of approximately 109 nm[Fig. 8(A) and (B)]. Aberration-corrected high-angle annular dark-field scanning transmission electron microscope(HAADF-STEM) and elemental mapping confirmed the homogeneous distribution of Cr, Ru, and B, with their contents largely consistent with the initial feeding ratio[Fig. 8(C) and (D)]. X-ray absorption near-edge structure(XANES) spectra indicated a valence state close to +4 for Ru and an oxidation state tending towards +3 for Cr[Fig. 8(E) and (F)]. Wavelet transform extended X-ray absorption fine structure(WT-EXAFS) analysis revealed signals corresponding to Ru—O/B, Ru—(B)—Cr, Cr—O/B, Cr—(O)—Ru, and Ru—(O)—Ru bonds[Fig. 8(G) and (H)], providing direct evidence for the B-bridged coordination structure between Ru and Cr. Benefiting from the formed Ru—B—Cr structure, the catalyst exhibited outstanding activity, requiring overpotentials of only 205 mV for HER and 379 mV for OER to reach a current density of 1 A/cm^2. *In-situ* differential electrochemical mass spectrometry(DEMS) confirmed that the OER follows the adsorbate evolution mechanism(AEM) pathway[Fig. 8(I)—(K)]. Within the AEM, the formation of the OOH^* intermediate is the RDS. As shown in Fig. 8(L), the catalyst with the Ru—B—Cr structure exhibited the lowest energy barrier for OOH^* formation, indicating effective optimization of the adsorption energy on the Ru sites, thereby enhancing acidic OER performance. Furthermore, when evaluated

using the descriptors $-\eta_{OER}$ and $\Delta G_{O^*}-\Delta G_{OH^*}$, the catalyst was positioned near the peak of the volcano plot [Fig.8(M)], further corroborating its promotion effect on acidic OER. Leveraging the excellent bifunctional HER/OER activity, we assembled a proton exchange membrane(PEM) electrolyzer, which required a cell voltage of only 1.78 V at 1 A/cm^2, demonstrating promising application potential.

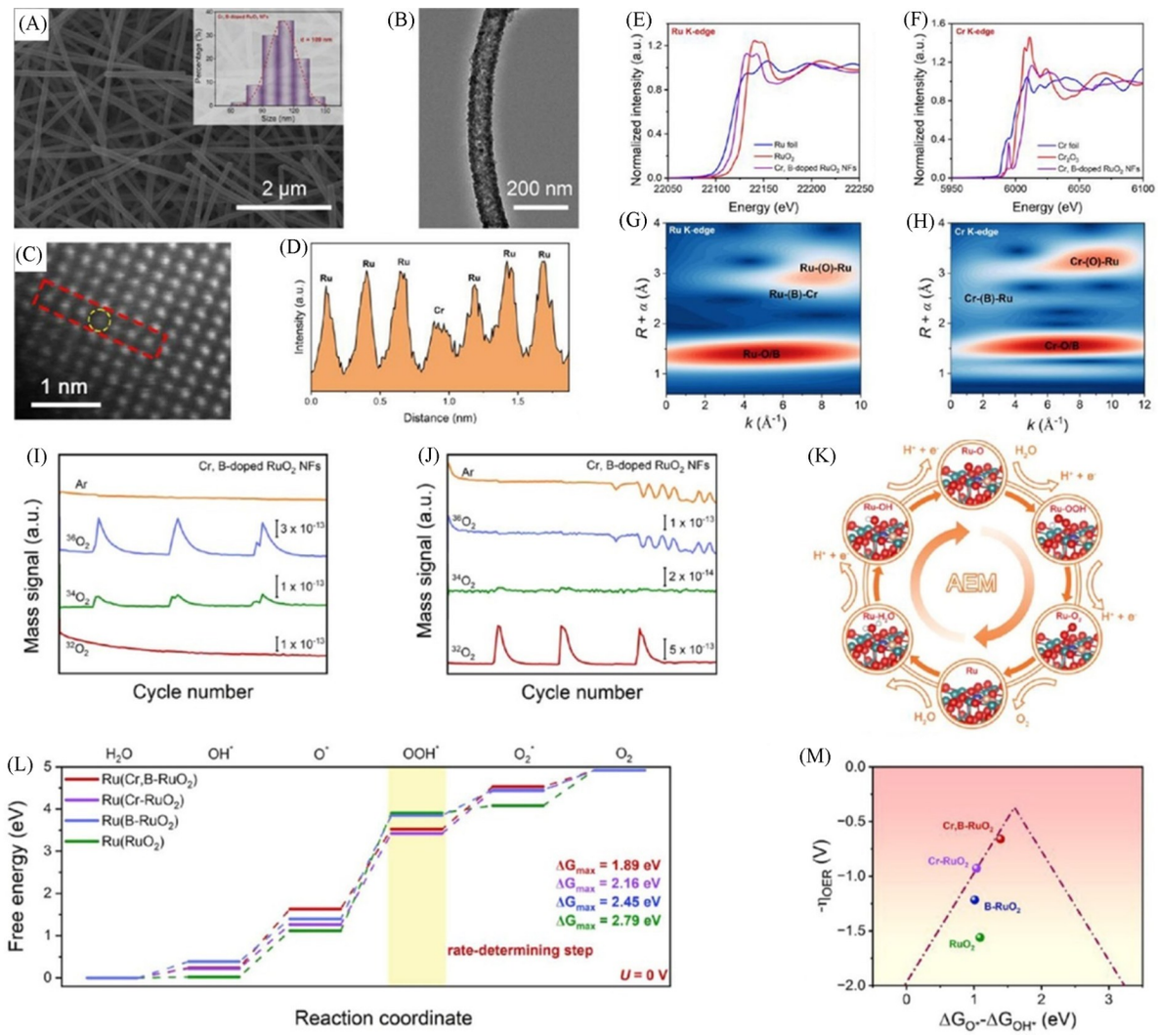


Fig. 8 SEM image(A), TEM image(B), magnified spherical aberration-corrected HAADF-STEM image (C) and corresponding line scanning intensity profile of Cr, B-doped RuO_2 NFs(D), XANES spectra for Ru K-edge(E) and Cr K-edge(F) for various samples, wavelet-transform EXAFS analysis at the Ru K-edge(G) and the Cr K-edge(H) of Cr, B-doped RuO_2 NFs, operando DEMS spectra for Cr, B-doped RuO_2 NFs using $H_2{}^{18}O$ solvent(I) and ^{18}O-labeled Cr, B-doped RuO_2 NFs with $H_2{}^{16}O$ solvent (J), schematic diagram of AEM mechanism for OER(K), free energy diagram of OER on various Ru sites(L) and correlation between the calculated negative overpotential($-\eta_{OER}$) and the descriptor of $\Delta G_{O^*}-\Delta G_{OH^*}$ for various catalysts(M)[67]

Copyright 2025, American Chemical Society.

4.4 Construction Strategies for Single-atom Catalysts

Single-atom catalysts(SACs) represent a class of high-performance catalysts where metal atoms are stabilized as isolated sites dispersed on the support material. These catalysts exhibit exceptional catalytic activity and stability due to their 100% atom utilization, structurally uniform active sites, and precisely tunable electronic structures[9,68]. Among the first-row transition metals, M—N—C catalysts typically feature

well-defined M—N_4 coordination sites as their active centers. This structure not only possesses unique electronic properties but also demonstrates outstanding catalytic performance. Furthermore, the interaction between the M—N_4 site and the carbon support can further modulate the local electronic environment, thereby optimizing the adsorption behavior of reaction intermediates and enhancing the overall catalytic performance.

Recently, a cobalt single-atom catalyst (Co SAs) anchored on nitrogen-phosphorus co-doped porous C NFs was successfully synthesized *via* a combined strategy of electrospinning, high-temperature carbonization, and acid etching. This material was employed as a self-supported bifunctional electrode for OWS[69]. The catalyst possessed a rich mesoporous structure with a high specific surface area of 654 m^2/g. XANES analysis indicated a Co—N(O) coordination environment for the Co species. The appearance of a characteristic peak at *ca.* 0.18 nm in the FT-EXAFS spectrum further confirmed the existence of the Co—N(O) coordination structure. EXAFS fitting results revealed that the central Co atom is coordinated by four N atoms and one O atom. This specific coordination structure effectively inhibits metal leaching, enhancing the material's stability. In terms of electrocatalytic performance, the catalyst exhibited an OER overpotential of 390 mV at 10 mA/cm^2 in alkaline medium. For the HER, it required low overpotentials of only 61 mV in acidic medium and 89 mV in alkaline medium at the same current density. DFT calculations demonstrated that P doping modulates the orbital electronic structure of the metal center, lowering the reaction free energy barriers for key intermediates on the M-N_4/O sites, thereby synergistically enhancing the kinetics of both HER and OER. When configured into a two-electrode OWS device, it required a cell voltage of only 1.68 V to achieve 10 mA/cm^2 and demonstrated stable operation for 10 h in alkaline conditions, showcasing promising catalytic activity and durability.

5 Conclusion and Perspectives

The development of low-cost, highly active bifunctional catalysts for both HER and OER is of paramount importance for advancing the practical application of water electrolysis for H_2 production. In recent years, electrocatalysts based on transition metals and their compounds (*e.g.*, oxides, phosphides, sulfides, and carbides) have been extensively investigated as promising alternatives to expensive and scarce noble-metal-based materials for various water electrolysis systems. Electrospinning, as a versatile nanomaterial fabrication technique, has been widely employed to construct transition metal-based electrocatalysts with tailored properties such as heterogeneous interfaces, core-shell structures, and precise doping, owing to its outstanding capability in manipulating micro-morphology and hierarchical architectures. Concurrently, it provides a flexible and reliable synthetic pathway for designing a large variety of composite materials for electrocatalytic applications.

This review has systematically summarized recent research progress in transition metal-based catalysts fabricated *via* electrospinning for electrocatalytic water splitting, with a particular focus on performance optimization strategies and material modification approaches for both HER and OER. Research demonstrates that through precise structural design and electronic structure modulation, various electrospun NFs-based transition metal catalysts have achieved remarkable enhancements in both catalytic activity and stability. To address key challenges such as sluggish reaction kinetics and insufficient adsorption/desorption capabilities of intermediates, strategies including heterostructure construction, heteroatom doping, metal-nonmetal-metal bridge bonding, and single-atom catalyst design have been developed, effectively boosting the intrinsic catalytic activity and reaction efficiency of the materials. Nevertheless, this field still faces several formidable challenges:

(1) Currently, although most transition metal-based bifunctional HER/OER catalysts demonstrate

excellent activity in alkaline media, material systems exhibiting efficient bifunctional performance in acidic or neutral environments remain relatively scarce, severely limiting their technological applicability. Future research must focus on developing transition metal-based materials that maintain high catalytic activity across a broad pH range (acidic, neutral, and alkaline) to expand their applications in various technological scenarios, such as PEM and anion exchange membrane electrolyzers.

(2) Under high current densities and prolonged operation, transition metal-based catalysts often suffer from issues like active species dissolution, structural collapse, or phase transformation, leading to significant performance degradation. This severely hinders their large-scale application in practical electrolyzers. Enhancing structural stability and corrosion resistance under harsh operating conditions requires systematic optimization at multiple scales, including composition and structure control, interface engineering, and electronic structure modification. The synergistic effect of these strategies can significantly improve catalyst durability at high current densities, ensuring long-term operation in industrial-grade water electrolysis devices.

(3) Most current studies still evaluate catalyst performance based on idealized three-electrode systems, which differ significantly from the operating environments of practical devices like PEM and anion exchange membrane electrolyzers. The lack of systematic evaluation, including long-term durability data under real electrolysis conditions, full-cell polarization curves, FE, and energy efficiency, makes it difficult to fully validate the practical performance and reliability of catalysts. This gap seriously impedes their transition from laboratory research to industrial application. Future work should emphasize comprehensive validation under realistic electrolysis conditions to accelerate the practical deployment of green hydrogen technology.

(4) Since the theoretical potential for the anodic OER is 1.23 V, a significant reduction in the overall energy consumption of water electrolysis is inherently challenging. Employing alternative small-molecule oxidation reactions to replace the OER presents a promising strategy to improve the efficiency of electrocatalytic H_2 production. This approach not only minimizes energy consumption but also enables the simultaneous synthesis of high-value chemicals or pollutant degradation at the anode[70—72]. However, such systems face challenges, particularly the need to synchronously optimize active sites for both the selective oxidation of small molecules and the HER to avoid competitive side reactions. Furthermore, in-depth exploration of reactant mass transfer and product separation in integrated systems is required.

In summary, electrospun nanofibrous transition metal-based electrocatalysts remain a crucial direction in water electrolysis research. Addressing the aforementioned challenges necessitates the development of these catalysts with higher activity and superior stability. This effort is essential to advance water electrolysis technology towards higher efficiency, cogeneration capabilities, and lower energy consumption, ultimately contributing to a sustainable energy future.

References

[1] Zhang J., Fu X., Kwon S., Chen K., Liu X., Yang J., Sun H., Wang Y., Uchiyama T., Uchimoto Y., Li S., Li Y., Fan X., Chen G., Xia F., Wu J., Li Y., Yue Q., Qiao L., Su D., Zhou H., Goddard W., Kang Y., *Science*, **2025**, *387*, 48—55
[2] Xia T., Ren Q., Yang J., Li Z., Shao M., Duan X., *Chem. Res. Chinese Universities*, **2024**, *40*, 577—589
[3] Quan L., Jiang H., Mei G., Sun Y., You B., *Chem. Rev.*, **2024**, *124*, 3694—3812
[4] Zhou Y., Yu W., Liu H., Fan R., Han G., Dong B., Chai Y., *EcoEnergy*, **2023**, *1*, 425—436
[5] Li W., Wang C., Lu X., *J. Mater. Chem. A*, **2021**, *9*, 3786—3827
[6] Cao X., Wang T., Jiao L., *Adv. Fiber Mater.*, **2021**, *3*, 210—228
[7] Song W., Li M., Wang C., Lu X., *Carbon Energ.*, **2021**, *3*, 101—128
[8] Song N., Ren S., Zhang Y., Wang C., Lu X., *Adv. Funct. Mater.*, **2022**, *32*, 2204751
[9] Shi B., Lu X., *Chem. Sci.*, **2025**, *16*, 17568—17594
[10] Wang C., Wang W., Qi H., Dai Y., Jiang S., Ding B., Wang X., Li C., Zeng J., Wu T., Li H., Wang Y., Zhao Y., Wang W., Li Z., Mo X., Hou H., Dong L., Ma H., Liu Y., Su C., Bai J., Wu W., Guo G., Nie G., Wang N., Zhu H., Bai J., Fang J., Liang D., Ba Z.,

Han G., Lu X., Wang K., Zhang X., Kang W., Deng N., Hu W., Chen W., Zhang X., Yang D., Wang F., Bian Y., Liu Z., Zhang L., Li X., Li L., Li Y., Huang H., Jia X., Li X., Yang D., Jin X., Li S., Zhang X., Tang N., Hao R., Tian F., Mai L., Wei Y., Xue J., *Prog. Mater. Sci.*, **2025**, *154*, 101494
[11] Zhu Y., Tang Z., Yuan L., Li B., Shao Z., Guo W., *Chem. Soc. Rev.*, **2025**, *54*, 1027—1092
[12] Fu X., Shi R., Jiao S., Li M., Li Q., *J. Energy Chem.*, **2022**, *70*, 129—153
[13] Lu X., Li M., Wang H., Wang C., *Inorg. Chem. Front.*, **2019**, *6*, 3012—3040
[14] Ni J., Shi Z., Wang Y., Yang J., Wu H., Wang P., Xiao M., Liu C., Xing W., *eScience*, **2025**, *5*, 100295
[15] Gao X., Chen Y., Wang Y., Zhao L., Zhao X., Du J., Wu H., Chen A., *Nano-Micro Lett.*, **2024**, *16*, 237
[16] Ghouri Z. K., Badreldin A., Ehaled K., Kumar D., Youssef K., Abdel-Wahab A., *J. Ind. Eng. Chem.*, **2021**, *96*, 243—253
[17] Chen J., Chen J., Yu D., Zhang M., Zhu H., Du M., *Electrochim. Acta*, **2017**, *246*, 17—26
[18] Li T., Li S., Liu Q., Yin J., Sun D., Zhang M., Xu L., Tang Y., Zhang Y., *Adv. Sci.*, **2020**, *7*, 1902371
[19] Liu X., Zhang M., Yang T., Wan L., Zhu H., Wang S., Du M., *Mater. Des.*, **2016**, *109*, 162—170
[20] Gebremariam T. T., Chen F., Jin Y., Wang Q., Wang J., Wang J., *Catal. Sci. Technol.*, **2019**, *9*, 2532—2542
[21] Wang L., Wang C., Mu Y., Fan J., Yang X., Yu C., Guo B., Zeng G., *Fuel*, **2025**, *391*, 134800
[22] Kwon T., Yu A., Kim S. J.,Kim M. H., Lee C., Lee Y., *Appl. Surf. Sci.*, **2021**, *563*, 150293
[23] Li W., Li M., Wang C., Lu X., *Sci. China Mater.*, **2023**, *66(3)*, 1024—1032
[24] Zhang B., Shan J., Yu J., Wang W., Li W., Li N., Li Y., *Int. J. Hydrog. Energy*, **2021**, *46*, 8871—8884
[25] Hua B., Li M., Zhang Y., Sun Y., Luo J., *Adv. Energy Mater.*, **2017**, *7*, 1700666
[26] Yu X., Qi R., Zhang L., Deng L., Zhong M., Chen Z., Lu X., *Acta Mater.*, **2025**, *294*, 121165
[27] Ding M., Wei Z., Zhao W., Lu Q., Lu C., Zhou M., Liu D., Yang H., *Green Chem.*, **2024**, *26*, 7789—7798
[28] Cao M., Li B., Cao Y., Li Y., Tian R., Shen Q., Xie W., Gu W., *ACS Appl. Mater. Interfaces*, **2025**, *17*, 15259—15273
[29] Huang T., Xu G., Ding H., Liu X., Zhang L., *Sep. Purif. Technol.*, **2025**, *354*, 129094.
[30] Huang T., Xu G., Ding H., Zhang L., Wei B., Liu X., *J. Colloid Interface Sci.*, **2022**, *625*, 956—964
[31] Chang X., Yan J., Ding X., Jia Y., Li S., Zhang M., *Nanomaterials*, **2022**, *12*, 3886
[32] Xie X., Liu J., Gu C., Li J., Zhao Y., Liu C., *J. Energy Chem.*, **2022**, *64*, 503—510
[33] Chen J., Huang F., Ke S., Shen J., Li Y., Zheng F., Li S., *Dalton Trans.*, **2022**, *51*, 5168—5174
[34] Liu X., Xu G., Ding H., Zhang L., Huang T., *Int. J. Hydrogen Energy*, **2023**, *48*, 35064—35074
[35] Meng D., Ran S., Gao L., Zhang Y., San X., Zhang L., Li R., Jin Q., *Chem. Res. Chinese Universities*, **2024**, *40*, 490—498
[36] Wang F., Xu L., Wang P., Zhang Y., *Electrochim. Acta*, **2019**, *306*, 437—445
[37] Li W., Zhong M., Chen X., Ren S., Yan S., Wang C., Lu X., *Sci. China Mater.*, **2023**, *66*, 2235—2245
[38] Shah M., Jang G., Zhang K., Park J., *EcoEnergy*, **2023**, *1*, 344—374
[39] Xu S., Sun X., Cui W., Bai J., Li C., *Int. J. Hydrogen Energy*, **2024**, *49*, 309—321
[40] Zhang J., Sun X., Peng W., Lu G., Sun S., Xu Y., Fang C., Li Q., Han J., *ChemCatChem*, **2020**, *12*, 3737—3745
[41] Li M., Zhu Y., Wang H., Wang C., Pinna N., Lu X., *Adv. Energy Mater.*, **2019**, *9*, 1803185
[42] Zhang S., Le F., Jia W., Yang X., Hu P., Wu X., Shu W., Xie Y., Xiao W., Jia D., *Small Methods*, **2025**, *9*, 2401103
[43] Zhang W., Yang L., Li Z., Nie G., Cao X., Fang Z., Wang X., Ramakrishna S., Long Y., Jiao L., *Angew. Chem. Int. Ed.*, **2024**, *63*, e202400888
[44] Zhang X., Liang Z., Zhang X., Guo Q., Xie Y., Wang L., Fu H., *Chin. Chem. Lett.*, **2025**, *36*, 109935
[45] Kumar M. R., Thiruvengadam D., Kumar K. S., Rajan K., Jayabharathi J., Padmavathy M., *Energy Fuels*, **2025**, *39*, 6605—6619
[46] Xia M., Shi B., Li W., Yu X., Qi R., Mu M., Wang C., Lu X., *J. Colloid Interface Sci.*, **2026**, *702*, 138880
[47] Zhong M., Yan S., Xu J., Wang C., Lu X., *Inorg. Chem. Front.*, **2022**, *9*, 4881—4891
[48] Nagappan S., Minhas H., Urkude R. R., Pathak B., Kundu S., *Small*, **2025**, *21*, 2500081
[49] Nagappan S., Jayan R., Rajagopal N., Krishnan A., Islam M. M., Kundu S., *Small*, **2024**, *20*, 2403908
[50] Gong T., Zhang J., Liu Y., Hou L., Deng J., Yuan C., *Chem. Eng. J.*, **2023**, *451*, 139025
[51] Cui W., Sun X., Xu S., Li C., Bai J., *Sustain. Energy Fuels*, **2024**, *8*, 4962
[52] Zhang Y., Shi W., Bo L., Shen Y., Ji X., Xia L., Guan X., Wang Y., Tong J., *Chem. Eng. J.*, **2022**, *431*, 134188
[53] Thiruvengadam D., Nithiasri R., Sangamithirai M., Kumar K. S., Jayabharathi J., *ACS Appl. Energy Mater.*, **2025**, *8*, 1266—1281
[54] Li T., Yin J., Sun D., Zhang M., Pang H., Xu L., Zhang Y., Yang J., Tang Y., Xue J., *Small*, **2022**, *18*, 2106592
[55] Li W., Guo W., Zhang L., Zhong M., Ren S., Yu G., Wang C., Chen W., Lu X., *Chem. Sci.*, **2024**, *15*, 11890—11901
[56] Zhao X., Liu M., Shang Z., Lu Q., Han X., Ji X., Zhang H., *Energy Fuels*, **2024**, *38*, 17939—17947
[57] Zhu H., Zhang J., Yanzhang R., Du M., Wang Q., Gao G., Wu J., Wu G., Zhang M., Liu B., Yao J., Zhang X., *Adv. Mater.*, **2015**, *27*, 4752—4759
[58] Wang T., Shi Y., Fei J., Zhu J., Song L., Li C., Zhan T., Lai J., Wang L., *App. Catal. B: Environ.*, **2024**, *358*, 124367
[59] Chae S. H., Muthurasu A., Kim T., Kim J. S.,Khil M. S., Lee M., Kim H., Lee J. Y.,Kim H. Y., *Appl. Catal. B: Environ.*, **2021**, *293*, 120209
[60] Yu X., Zhang L., Qi R., Xia M., Wang Y., Zhong M., Song W., Lu X., *J. Colloid Interface Sci.*, **2025**, *699*, 138225

[61] Li W., Liu R., Yu G., Chen X., Yan S., Ren S., Chen J., Chen W., Wang C., Lu X., *Small*, **2024**, *20*, 2307164
[62] Zhang L., Li W., Ren S., Song W., Wang C., Lu X., *Adv. Energy Mater.*, **2025**, *15*, 2403136
[63] Surendran S., Jesudass S. C., Janani G., Kim J. Y., Lim Y., Park J., Han M. K., Cho I. S., Sim U., *Adv. Mater. Technol.*, **2023**, *8*, 2200572
[64] Wang X., Chen X., Huang M., Liu Z., *Int. J. Hydrogen Energy*, **2024**, *63*, 556—565
[65] Li W., Wang C., Lu X., *Nano Lett.*, **2024**, *24*, 11779—11792
[66] Li Y., Zhou B., Ding W., Luo Q., Wang L., Kim I., Zhang T., Ji D., Qin X., *Appl. Catal. B: Environ. Energy*, **2025**, *380*, 125776
[67] Li W., Zhang L., Ma L., Wang J., Qi R., Pang Y., Xu C., Wang C., Gao M., Lu X., *Nano Lett.*, **2025**, *25*, 443—452
[68] Yu J., Li J., Xu C., Li Q., Liu Q., Liu J., Chen R., Zhu J., Wang J., *Nano Energy*, **2022**, *98*, 107266
[69] Li J., Zhu J., Jia Z., Li R., Yu J., *Chem. Asian J.*, **2023**, *18*, e202300393
[70] Wang Y., Jiang Q., Ren S., Xu J., Wang Y., Zhong M., Lu X., *Adv. Mater.*, **2025**, *37*, 2504922
[71] Xu M., Xu J., Zhang L., Yu X., Ren S., Zhang S., Gao M., Zhong M., Lu X., *Adv. Energy Mater.*, **2025**, 15, e01970
[72] Zhong M., Xu M., Ren S., Li W., Wang C., Gao M., Lu X., *Energy Environ. Sci.*, **2024**, *17*, 1984—1996

(Ed.: F, K, S)